Journal of Natural Gas Science and Engineering 96 (2021) 104289

Contents lists available at ScienceDirect

Journal of Natural Gas Science and Engineering

journal homepage: www.elsevier.com/locate/jngse

A review of the features and applications of ZIF-8 and its derivatives for separating CO_2 and isomers of C_3- and C_4- hydrocarbons

Manel Bergaoui [a,b], Mohamed Khalfaoui [a,b], Ahmed Awadallah-F [c,1], Shaheen Al-Muhtaseb [c,*]

[a] Research Group in Materials Science, Microelectronics and Nanotechnologies, Department of Technology, Higher Institute of Computer Sciences and Mathematics of Monastir, University of Monastir, Monastir, 5000, Tunisia
[b] Laboratory of Physical Chemistry of Materials, Department of Physics, Faculty of Sciences, University of Monastir, Monastir, 5000, Tunisia
[c] Department of Chemical Engineering, Qatar University, P.O. Box 2713, Doha, Qatar

ARTICLE INFO

Keywords:
Zeolitic imidazolate frameworks (ZIFs)
Synthesis
Characteristics
Gas separation
Gate opening
Statistical physics

ABSTRACT

Metal organic framework (MOF) membranes have gained more attentions due to their abilities in various applications in gas and liquid separations. The majority of works are related to Zeolite imidazolate frameworks-8 (ZIF-8). This is often attributed to its high stability, easy synthesis, and good gas separation. They have gained a significant interest of scientists and have the aptitude to be utilized in other gas separations and applications. Indeed, the investigation of the literatures revealed that ZIF-8 and its derivatives have a substantial attention due to of its good properties as its large specific surface area, "gate opening" mechanism, etc …, which makes them special in adsorption/membrane separations and other associated aspects. The applications of ZIF-8 based materials for carbon dioxide (CO_2) gas adsorption and the C_3- and C_4- isomers' (propane, propylene, n-butane and isobutane) gas separation also are discussed. Statistical physics approach was applied throughout this review as a perfect tool to discuss and understand properties of ZIF-8, especially the "gate opening pressure". Subsequently, this review points to present highlights and applications of ZIF-8 and its derivatives for the purpose of carbon dioxide and hydrocarbon separations. Additionally, this study considers recent advancements of ZIF-8 synthesis and prospects for its use in gas separation. This study can help to better understand effective features of a sorbent and methods for gas separation process. As theoretical discussions are referred to as a crucial issue, this is the first study on Zeolitic Imidazolate Framework (ZIF) membrane application, which provides the use of statistical physics theoretical approach and considers the effect of nanogate opening pressures.

1. Introduction

In recent years, zeolitic imidazolate frameworks (ZIFs) have developed rapidly. Their structures are generated according to tetrahedral units where every metal ion (M) attaches to four organic imidazolate (Im) linkers (M−Im−M). Indeed, ZIFs are considered as a sub-family of MOFs, and their topology has been similar to that of zeolites (Song et al., 2012). ZIFs combine the advantages of both MOFs and zeolites since they have properties of these two materials such as crystallinity, porosity, and enthralling chemical and thermal stability (Sankar et al., 2019; Zou et al., 2018a). Moreover, ZIFs are considered as attractive candidates for several applications in gas separation by adsorption or in membranes, in sensing and in catalysis (Chen and Wang, 2020; Matsuoka et al., 2018; Samadi-Maybodi et al., 2015; Awadallah-F et al., 2019a). This advantage was ascribed to their excellent properties, including their high surface areas, microporous structures, chemical and thermal stabilities (Park et al., 2006); and synthesis controllability due to their structural flexibility, which leads to a sensible design of both their pore sizes and surface functionality. Therefore, special properties and applications of the ZIF family are under heavy research, where zeolitic imidazolate framework-8 (ZIF-8) is the most popular and classic member of this family. An advantage of ZIF-8 nanoparticles is their excellent stability that enabled long term operation (Yuan et al., 2017).

Zeolitic imidazolate framework-8 (ZIF-8) ($Zn(mIm)_2$, where mIm is the 2-methylimidazolate) displays a solidate (SOD) topology (Fig. 1) that features a space group of interconnected six membered ring

* Corresponding author.
E-mail addresses: manelbergaouitn@gmail.com (M. Bergaoui), s.almuhtaseb@qu.edu.qa (S. Al-Muhtaseb).
[1] Current address: Radiation Research of Polymer Department, National Centre for Radiation Research and Technology, Atomic Energy Authority, P.O. Box 29, Nasr City, Cairo, Egypt.

https://doi.org/10.1016/j.jngse.2021.104289
Received 11 June 2021; Received in revised form 16 September 2021; Accepted 7 October 2021
Available online 9 October 2021

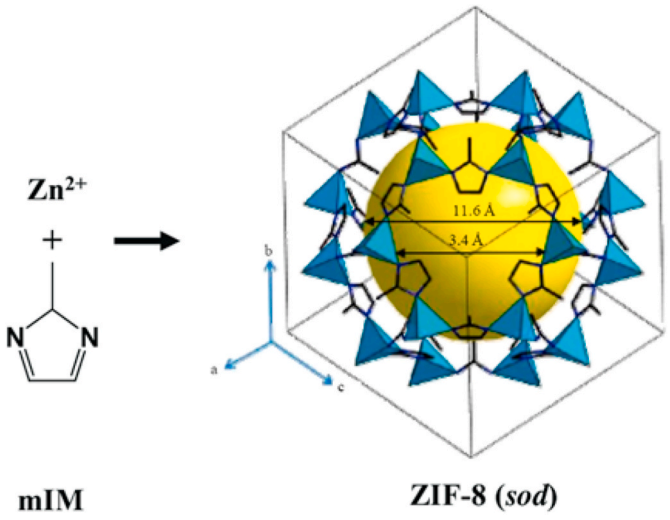

Fig. 1. Three-dimensional structure of ZIF-8 in cubic unit cell at 111 plane, Zn (polyhedral), N (sphere), and C (line)) (Park et al., 2006; Banerjee et al., 2008; Sze Lai et al., 2014a).

windows with an accessible diameter and pore width of 3.4 Å and 11.6 Å, respectively (Park et al., 2006; Banerjee et al., 2008; Sze Lai et al., 2014a). ZIF-8 contains 276 atoms in each unit cell. It crystallizes in cubic space group $I\bar{4}3m$ with a lattice constant of 16.992 Å (Awadallah-F et al., 2019a; Huang et al., 2006). ZIF8 and its derivatives have a highly stable structure and play an important role in promising membranes for gas separation processes. Due to its robustness and good separation ability, many researchers have conducted further studies on it. (Song et al., 2012; Awadallah-F et al., 2019a; Awadallah-F et al., 2019b; Awadallah-F et al., 2019c).

Recent advancements in the chemical and petrochemical industries led to the development of various methods and technologies for gas separation. Due to its widespread use, the global demand for high-purity gas is growing rapidly. Gas separation has a potential impact on the chemical processing industry. Therefore, many separation processes and techniques have been used for gas separation. Table 1 summarizes the most important methods and points out their advantages and disadvantages. The innovation of gas separation through adsorption technology is related to the discovery of new adsorbents, such as organometallic frameworks (MOFs), especially zeolite imidazole frameworks (ZIFs), which have excellent thermal and chemical stability, and have microporous voids, leading to the large-scale industrial application of ZIFs (Wang et al., 2016; Neelakanda et al., 2016; Melgar et al., 2015; Bernardo et al., 2009; Pullumbi et al., 2019; Wankat, 1991).

Table 1
Main technologies and methods of gas separation (Wang et al., 2016; Neelakanda et al., 2016; Melgar et al., 2015; Bernardo et al., 2009; Pullumbi et al., 2019; Wankat, 1991).

Separation method/ technology	Advantages	Disadvantages
Absorption by Solvents	High recovery rate of separation	• Degradation in the oxidizing environment • High amount of energy required for regeneration
Membrane Separations	• Many membranes are developed • Possibility to combine membranes with solvents	• Cannot achieve a high degree of separation • High energy consumption • Not widely used due to manufacturing challenges
Cryogenic Separations	Direct production of liquid CO_2 for example	High amount of energy is required for refrigeration
Adsorption	Easy regeneration	Low selectivity for some gases

Understanding how ZIF-8 interacts with alkanes is vital for its further development and commercialization in a wide range of applications. Applications of ZIF-8 materials are emerging due to their high porosity and stability, adjustable compositions and structural flexibility (Ma and Liu, 2019; Zou et al., 2018b). Both pristine ZIF-8 and its derivatives were developed as multifunctional materials making them attractive candidates for various applications such as environment protection (Pillai et al., 2019; Chen et al., 2019; Yoo et al., 2020), separations (Matsuoka et al., 2018); (Awadallah-F et al., 2019a; Awadallah-F et al., 2019b; Awadallah-F et al., 2019c), catalysis (Chen and Wang, 2020; Payra et al., 2020), sensing (Samadi-Maybodi et al., 2015), electronics (Aboraia et al., 2020) and drug delivery (Chen et al., 2018). In this section, attention will be focused on the gas separation. Indeed, ZIF-8 materials have a high potential in gas separation due to their highly porous structure. Moreover, gas separation can be affected by several factors such as ZIF-8 nanoparticle characteristics; including pore sizes, chemical modification, loading percentage and structure and fabrication conditions (such as method, temperature, time, …etc.) (Gong et al., 2017).

In this review, we analyze and summarize the recent research developments of ZIF-8 materials and its derivatives as well as their applications, especially for CO_2 gas separation. This review consists of different aspects including synthesis procedures to generate ZIF-8 nanomaterials, common characterization techniques and a summary of their main applications in several significant areas. Finally, it gives the latest research on the hydrocarbon adsorption by ZIF-8 and doped ZIF-8, along with new correlations of their corresponding adsorption isotherms. The notion of gate-opening pressure (P_0) of ZIF-8 and its derivatives for the adsorption and separation of various gases was well discussed and evaluated basing on statistical physics approach. Indeed, the present review focuses not only on the experimental point of view of ZIF-8 and its derivatives as proved by other review works (Feng et al., 2021; Li et al., 2021; Chen et al., 2014; Sze Lai et al., 2014b), but it also highlights the theoretical approach applied to ZIFs. To the best of our knowledge, the statistical physics theoretical approach was applied for the first time on Zeolitic Imidazolate Framework (ZIF) membranes applications while attempting to consider the effect of nanogate opening pressures.

2. Synthesis

Great advances have been made in the synthesis methods of MOFs. Fig. 2 shows a timeline of the most popular synthetic methods qualified for the MOFs synthesis (Yaghi, 1997; Rubio-Martinez et al., 2017) that are applied until today (Lu et al., 2020; Fang et al., 2020). Nonetheless, the synthesis of MOFs is not restricted to these methods. Recently, Li et al. (2020) used an immersion deposition method for La@ZIF-8 synthesis. Likewise, ultrasound-assisted method was applied by Mahmoodi et al. (2019) for the synthesis of ZIF-8, CNT/Fe_2O_3/ZIF-8 and NH_2-CNT/Fe_2O_3/ZIF-8. Some synthetic methods described above such as microwave, solvothermal, sonochemical, solvent method, microfluidic, electrochemical and steam-assisted methods (Awadallah-F et al., 2019a; Cho et al., 2013; Fu et al., 2018; Shi et al., 2011; Biswal et al., 2013; Martinez Joaristi et al., 2012; Lucero et al., 2019; Xie et al., 2014) are summarized in Table 2. In fact, compared with the solvothermal method, the method of first synthesizing the zeolite imidazole ester

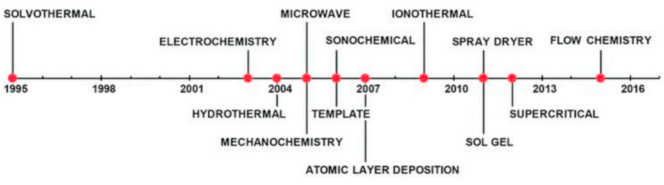

Fig. 2. Timeline of the most common synthetic methods patented for the synthesis of MOFs (Yaghi, 1997; Rubio-Martinez et al., 2017).

Table 2
State-of-the-art synthesis approaches and properties of ZIF-8 and its derivatives.

	Synthesis method	Zn^{2+} (mmol)	MeIMa (mmol)	Synthetic condition		Particle size (*μm*)	S_{BET} (m^2/g)	Ref.
				Solvent	Conditions			
ZIF-8	Microwave	4.45	39.5	Methanol	60 °C, 24 h, 100 W	0.328	61.05	(Awadallah-F et al., 2019a)
$Cu^{a}_{10\%}$/ZIF-8		(4.45 - x)				0.222		
$Cu_{30\%}$/ZIF-8		(4.45 - x)				0.227		
ZIF-8	Solvothermal	2	2	DMF[b]	140 °C, 24 h	150–200	1370	(Lee et al., 2015)
	Microwave	2	2	DMF	120 °C, 3 h, 80 W	5–10	1250	
ZIF-8	Sonochemical	10	10	TEA[c] and NaOH[d]	300 W, 20 KHz	0.7	1253	(Cho et al., 2013)
ZIF-8	Solvent method	1.5	3	Methanol	1000 rpm, 60 °C	–	1410	(Fu et al., 2018)
PVP[e]: ZIF-8/CNTs[f]					1000 rpm, 60 °C, 0.1 g (PVP), 15 mg (CNTs)	0.47–1.9	945	
SDS[g]: ZIF-8/CNTs					1000 rpm, 60 °C, 0.1 g (PVP), 15 mg (CNTs)	0.13–0.42	976	
CTAB[h]: ZIF-8/CNTs					1000 rpm, 60 °C, 0.1 g (PVP), 15 mg (CNTs)	0.1–0.11	928	
ZIF-8	Microfluidic (T-mixer)	2.25	157.5	H_2O	10 min, 100 °C	0.3–0.9	1730 ± 14.7	Shi et al. (2011)
GQD@ZIF-8[i]	electrochemical	0.3	2.43	Methanol	Under vacuum, 6 h	0.036	983	Biswal et al. (2013)
ZIF-8	Steam-assisted	0.5	5	H_2O	120 °C, 24 h	–	1470	Martinez Joaristi et al. (2012)

x was varied from 0 to 2.23 to alter the ratio of $Cu(NO_3)_2{\cdot}2.5H_2O/Zn(NO_3)_2{\cdot}6H_2O$ into the solution.
[a] Copper.
[b] Dimethylformamide.
[c] Trimethylamine.
[d] Sodium hydroxide.
[e] Polyvinylpyrrolidone.
[f] Carbon nanotubes.
[g] Sodium dodecyl sulfate.
[h] Cetyltrimethylammonium bromide.
[i] Graphene quantum dots.

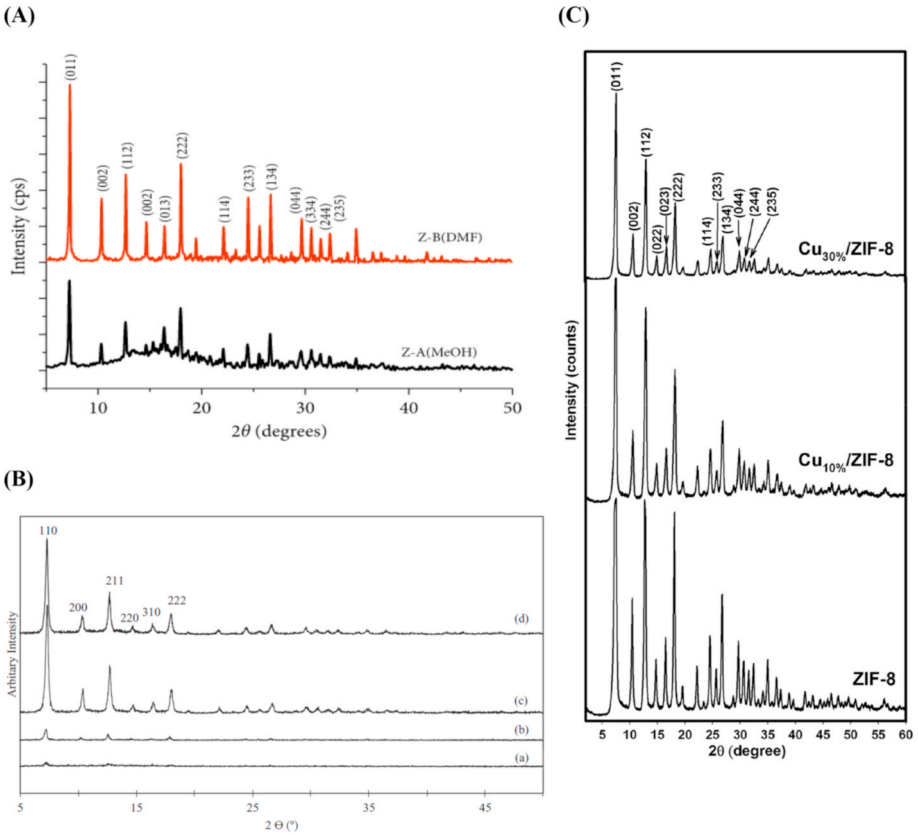

Fig. 3. XRD patterns of (A) Z-A(MeOH) and Z-B(DMF) samples (Du et al., 2019), (B) ZIF-8 samples synthesized at (a) 80 °C; (b) 100 °C; (c) 120 °C and (d) 140 °C within 0.5 h under microwave irradiation (Lai et al., 2016) and (C) ZIF-8, $Cu_{10\%}$/ZIF-8 and $Cu_{30\%}$/ZIF-8 samples (Awadallah-F et al., 2019a).

framework (ZIF) requires complicated and long steps (Park et al., 2006). Generally speaking, smaller and uniform crystals with a thinner size distribution have been discovered by microwave-assisted methods, which are very desirable for some useful applications (Lucero et al., 2019). Bao et al. (2013) shows that the samples produced by the hydrothermal method have irregular shapes and variable particle sizes. However, a homogeneous sample having a hexagonal shape and an average particle diameter of about 0.350 μm was obtained by the microwave radiation synthesis method. On the other hand, the average particle size is affected by other synthesis conditions, such as Zn:2MeIm molar ratio, solvent, reaction temperature, irradiation time, precursor concentration, pressure, and mixed metal content (Fu et al., 2018; Muñoz-Gil and Figueiredo, 2019; Dunne et al., 2015).

3. Common characterization techniques

Various techniques were used to characterize the synthesized ZIF8 material in the goal to study the structure, morphology, physico-chemical properties and thermal stability of the material.

3.1. Crystal structure prediction

The crystal structure and purity of ZIF8 can be demonstrated by characterization experiments using single crystal **X-ray** diffraction (XRD) methods. The high crystallinity of the produced ZIF8 material originates from the (001) very sharp peak at 2θ = 7.36°(Samadi-Maybodi et al., 2015; Li et al., 2019; Duan et al., 2020). Moreover, from the XRD pattern, the particle size distribution could be estimated based on Scherrer Equation (Lai et al., 2016). Fig. 3 (A) shows an X-ray diffraction analysis of ZIF-8 that was synthesized with methanol and dimethylformamide solvents as denoted, respectively, by Z-A(MeOH) and Z-B (DMF) (Du et al., 2019). Indeed, high crystallinity of both samples was deduced from the diffraction peak (011) at $2\theta = 7.36°$. However, Z-B (DMF) has higher symmetric planes since its diffraction peaks intensity is higher compared to those of Z-A(MeOH), which indicates the effect of solvent in ZIF-8 synthesis. On the other hand, Lai et al. (2016) have studied the temperature effect from 80 °C to 140 °C, where XRD characterization leads to detecting the higher crystallinity of ZIF-8 synthesized at 120 °C and 140 °C (Fig. 3 (B)). Indeed, to generate a supersaturation condition for the formation of ZIF-8 during a small period time (0.5 h), a lower temperature of 100 °C is insufficient, which led to the absence of its characteristic peak.

In addition, some studies have reported the synthesis of mixed metal/ligand ZIF (Chen et al., 2018; Kaur et al., 2016; Botas et al., 2010; Caskey et al., 2008; Zhang et al., 2019; Liu et al., 2019). Awadallah et al. (Awadallah-F et al., 2019a) have showed that similar XRD patterns was detected for both ZIF-8 and Cu/ZIF-8 (Fig. 3 (C)). This indicates that the crystal structure in the I43m space group is retained after ZIF8 doping.

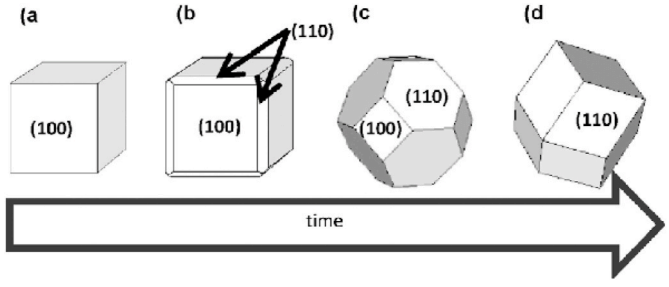

Fig. 4. Illustration of the crystal morphology evolution with time: (a) cube, (b) cube with truncated edges, (c) rhombic dodecahedron with truncated corners, and (d) rhombic dodecahedron (Schejn et al., 2014; Jing et al., 2020).

3.2. Size and morphology-controlled nanocrystals

Scanning electron microscope SEM imaging was used to study the morphology and crystal size distribution as a function of synthesis conditions. Indeed, as shown in Fig. 4, the development of ZIF-8 crystals was established by time progressing from cubes displaying 6 {100} faces to rhombic dodecahedra displaying 12 {110} faces. Probably, the latter is being the most stable ZIF-8 equilibrium morphology (Schejn et al., 2014; Jing et al., 2020).

Jian et al. (2015a) investigated the development of ZIF-8 crystals depending on synthesis time (Fig. 5 (A)). Bumpy spherical particle surfaces are detected at 5 min. The period that presents the metastable phase for ZIF-8 growth was achieved when time increasing to 20–60 min. Thereafter, crystals with heterogeneous hexagonal facets begin to display. Homogeneous surfaces with little defects were established for ZIF-8 crystals at 4 h. By increasing time up to 8 h, the formation of various little ZIF-8 crystallites was attained, whereas the quantity turned into trivial at 16 h. The mechanism of Ostwald ripening (Challa et al., 2011) allows to describe this phenomenon. The well-known typical morphology of ZIF-8 given by rhombic dodecahedron shape with 12 {011} surfaces was attended at 24 h. After 3 days, this equilibrium shape is preserved.

Jing et al. (2020) showed that the morphology and the average particle size changed with molar ratio of Ag/AgCl co-doped ZIF-8 as shown in Fig. 5 (B). Indeed, an average size of 600 ± 24 nm was found after 24 h of reaction time for ZIF-8 nanoparticles with a rhombic dodecahedron shape (Fig. 5a (B)). A reduction of the ZIF-8 particle size to 550 nm was detected by the addition of 5 mmol of $AgNO_3$ with a well-defined truncated rhombic dodecahedral crystals (Fig. 5b (B)). When 10 mmol of $AgNO_3$ is added, ZIF-8 average particle size decreased to 400 ± 18 nm. Thereafter, little Ag/AgCl nanoparticles are created in ZIF-8 nanomaterials (Fig. 5c (B)). For a 15 mmol of AgNO3, the average size decreased to 300 ± 22 nm with a well-defined shrunken cubic crystals (Fig. 5d (B)). Finally, when adding 20 mmol of $AgNO_3$, ZIF-8 particle size decreased to 200 ± 20 nm (Fig. 5e (B)). This same decrease of particle size has been also detected by Awadallah et al. (Awadallah-F et al., 2019a) in the case of Cu/ZIF-8, where the obtained nanocrystal size decreases following the increase of Cu^{2+} percentage (Fig. 5 (C)).

In addition, it has been observed that by changing the molar ratio of 2-methylimidazole (Hmim)/zinc nitrate hexahydrate (Zn), the morphology and average size can also be changed (Jian et al., 2015a; Kida et al., 2013; Tanaka et al., 2012). Zhang et al. (2018) shows that ZIF-8 synthesized with a Hmim/Zn molar ratio of 1 has a cubic shape with particles sizes of 0.4 μm and 0.8 μm. When the Hmim/Zn molar ratios are greater than unity, the morphology of all samples changes to truncated rhombic dodecahedron or rhombic dodecahedron shapes. Furthermore, a decrease of average particle size from 1.0 μm to 0.1 μm was detected by increasing the Hmim/Zn molar ratio from 4 to 16, respectively (Zhang et al., 2018).

3.3. Chemical characterizations

Functional groups: The presence of an imidazole group and a Zn–N interaction was confirmed by Fourier-transform infrared (FT-IR) spectra of ZIF-8, which confirms that the synthesis of ZIF-8 crystals was succeeded (Samadi-Maybodi et al., 2015; Du et al., 2019; Binaeian et al., 2019). Indeed, for pure ZIF-8, peaks at 2920–3180 cm^{-1} show the stretching of aliphatic and aromatic C–H of imidazole ring, respectively. The peaks for out-of-plane and in-plane bending of imidazole ring are below 800 cm^{-1} and in the region of 900–1350 cm^{-1}, respectively. The peak around 1600 cm^{-1} is due to the C═N stretch mode, while the sharp peaks at around 1300–1500 cm^{-1} were attributed to the stretching of the entire ring. Finally, the peak at 420 cm^{-1} shows the stretching of Zn–N bond when the zinc atoms in ZIF-8 connect to the nitrogen atoms of 2-methylimidazole linker during ZIF-8 synthesis (Samadi-Maybodi

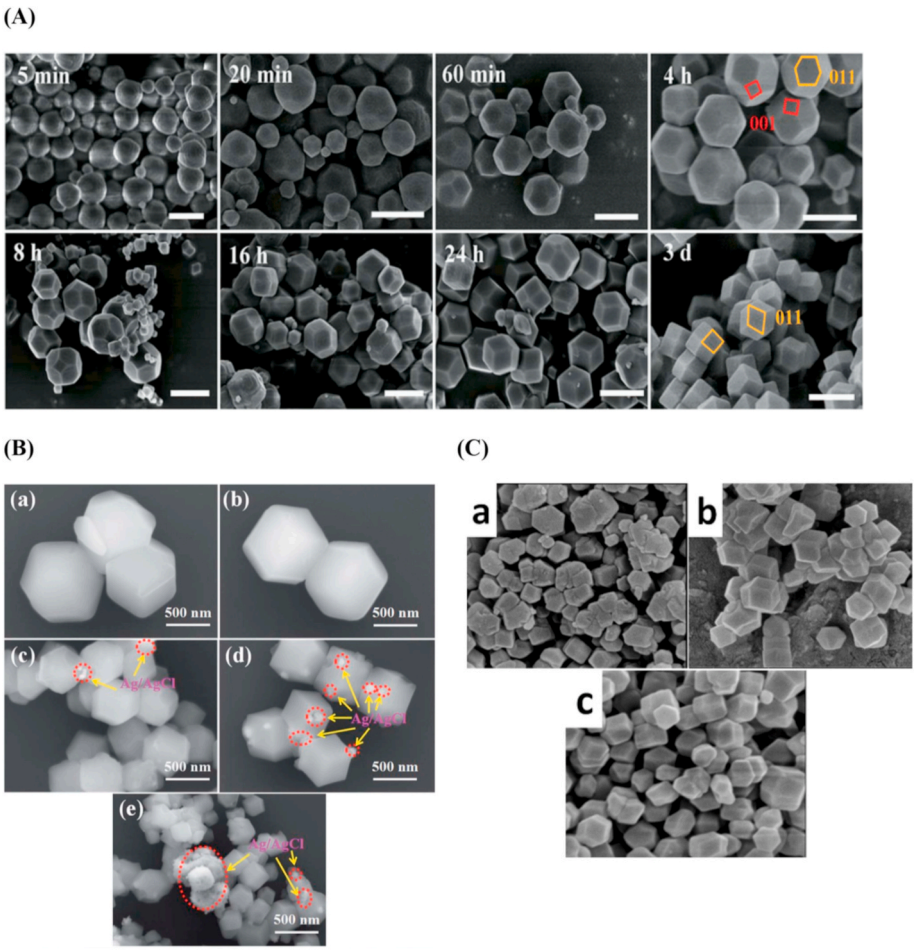

Fig. 5. (A) Shape evolution of synthesized ZIF-8 obtained from $Zn(OAc)_2$ in water as a function of reaction time with a Zn/Hmim/H_2O molar ratio of 1/35/1238 (Jian et al., 2015a). (B) SEM images of (a) ZIF-8, (b) Ag/AgCl(5)@ZIF-8, (c) Ag/AgCl(10)@ZIF-8, (d) Ag/AgCl(15)@ZIF-8 and (e) Ag/AgCl(20)@ZIF-8 (Jing et al., 2020). (C) SEM images of (a) ZIF-8, (b) $Cu_{10\%}$/ZIF-8 and (c) $Cu_{30\%}$/ZIF-8 (Awadallah-F et al., 2019a).

et al., 2015; Binaeian et al., 2019; Xu et al., 2019).

Fig. 6 (i) shows an example of ZIF-8 and Cu/ZIF-8 FTIR spectra (Awadallah-F et al., 2019a), where some peaks were shifted compared to 2-methylimidazole molecule. This finding leads to conclude that the final products of ZIF-8, $Cu_{10\%}$/ZIF-8 and $Cu_{30\%}$/ZIF-8 were created without leaving any remains of unreacted 2-methylimidazole (Awadallah-F et al., 2019a).

Raman spectra: Raman spectra give structural fingerprint of molecules. The standard Raman peaks for ZIF-8 and doped ZIF-8 materials are regrouped in Table 3 (Awadallah-F et al., 2019a; Pillai et al., 2019; Radhakrishnan and Narayana, 2016; Tanaka et al., 2015; Tsotsalas et al., 2016).

Surface Composition: Elemental composition and binding energy of ZIF-8 materials was analyzed by X-Ray photoelectron spectroscopy (XPS) analysis technique (Awadallah-F et al., 2019a; Liu et al., 2016; Chin et al., 2018). Fig. 6(iii) illustrates an example of whole XPS spectra of ZIF-8, $Cu_{10\%}$/ZIF-8 and $Cu_{30\%}$/ZIF-8 samples. Indeed, the results showed the presence of not only ZIF-8 framework elements (such as Zn, C, N and O) in ZIF-8 nanomaterials, but also Cu in the $Cu_{10\%}$/ZIF-8, and $Cu_{30\%}$/ZIF-8 samples. The binding energies of $Cu_{10\%}$/ZIF-8 and $Cu_{30\%}$/ZIF-8 samples was affected by the admission of Cu^{2+} into matrix where a shift to lower energy values was attained compared to ZIF-8 sample (Awadallah-F et al., 2019a).

3.4. Thermal stability analysis

The decomposition of samples with temperature was monitored using thermogravimetric analysis (TGA) that was carried out using a PerkinElmer Pyris6 TGA analyzer under a N_2 gas in the range of 150 °C–1000 °C with heating rate 10 °C/min. This technique is frequently used to identify the limits of materials' thermal stability (Howarth et al., 2016). For instance, Awadallah et al. (Awadallah-F et al., 2019a) showed that the thermal stability of ZIF-8 decreases with the presence of Cu^{2+} (Fig. 7). Moreover, no weight loss was detected at 150 °C, for ZIF-8 and $Cu_{10\%}$/ZIF-8, whereas $Cu_{30\%}$/ZIF-8 presents a weight loss of 1.49%. The weight loss at 514 °C for ZIF-8 is 4.88%; whereas for $Cu_{10\%}$/ZIF-8 and $Cu_{30\%}$/ZIF-8, this value becomes 5.48%. At 1000 °C, the weight loss of ZIF-8 is 74.75%; whereas for $Cu_{10\%}$/ZIF-8 and $Cu_{30\%}$/ZIF-8, the weight losses are 82.35%, and 66.53%, respectively (Awadallah-F et al., 2019a).

On the other hand, Schejn et al. (2015) also showed a similar trend where no weight loss was detected until 350 °C for adsorbents $Cu_{1\%}$/ZIF-8, $Cu_{5\%}$/ZIF-8, $Cu_{10\%}$/ZIF-8, $Cu_{25\%}$/ZIF-8; indicating good thermal stabilities for all samples. Thereafter, the order of thermal stability in the range of 350 °C–400 °C is $Cu_{1\%}$/ZIF-8 > $Cu_{5\%}$/ZIF-8 > $Cu_{10\%}$/ZIF-8 > $Cu_{25\%}$/ZIF-8. A sharp weight loss of 63–64% was detected when the temperature was raised from 400 to 500 °C; with the corresponding order: $Cu_{5\%}$/ZIF-8 > $Cu_{25\%}$/ZIF-8 > $Cu_{1\%}$/ZIF-8 > $Cu_{10\%}$/ZIF-8. Indeed, the difference in the ranges of temperature

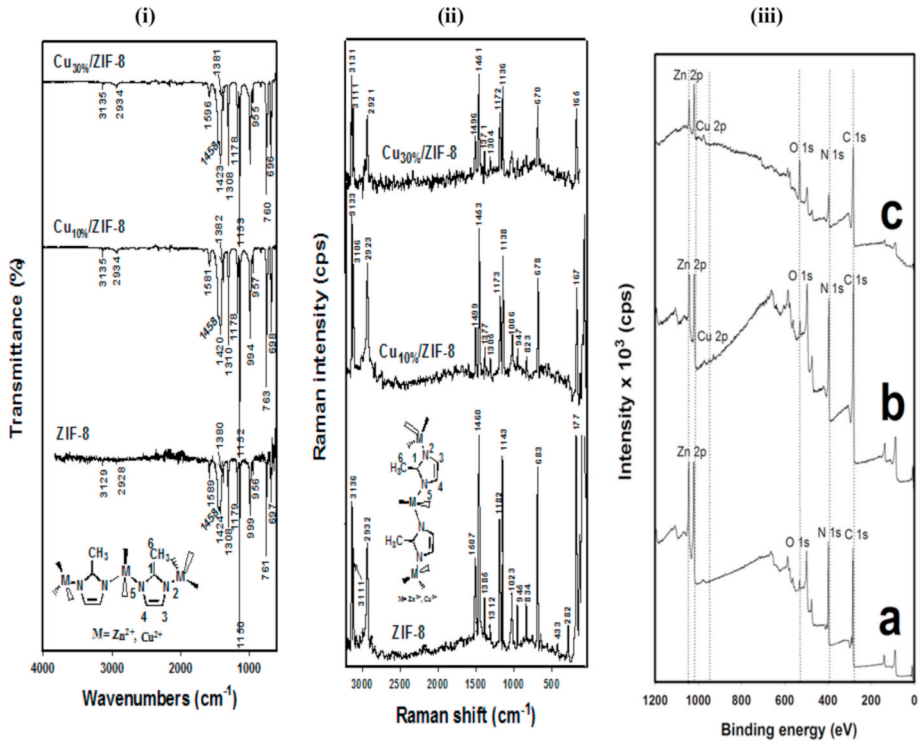

Fig. 6. (i) FTIR spectra, (ii) Raman spectra and (iii) XPS analysis of (a) ZIF-8, (b) $Cu_{10\%}$/ZIF-8 and (c) $Cu_{30\%}$/ZIF-8 adsorbents (Awadallah-F et al., 2019a).

Table 3
Standard Raman peaks for ZIF-8 and doped ZIF-8 materials.

Raman shift (cm^{-1})	Peak assignment
282	stretching Zn–N
686	imidazole ring puckering
755	C=N out of plane bend and bending N–H
833, 950, 1021	C–H out of plane bend
1146, 1187	stretching C–N
1311	ring expansion + N–H wag,
1384	bending CH_3
1455	C–H wag
1499	C–N, N–H wag
1508	stretching C–C
3111, 3136	stretching C–H (imidazolium ring)

In the Raman spectra of ZIF-8 and Cu/ZIF-8 (Fig. 6(ii)), standard peaks for ZIF-8 material were observed (Awadallah-F et al., 2019a). Indeed, the shift of some peaks compared to the 2-methylimidazole molecule confirms the formation of the final product.

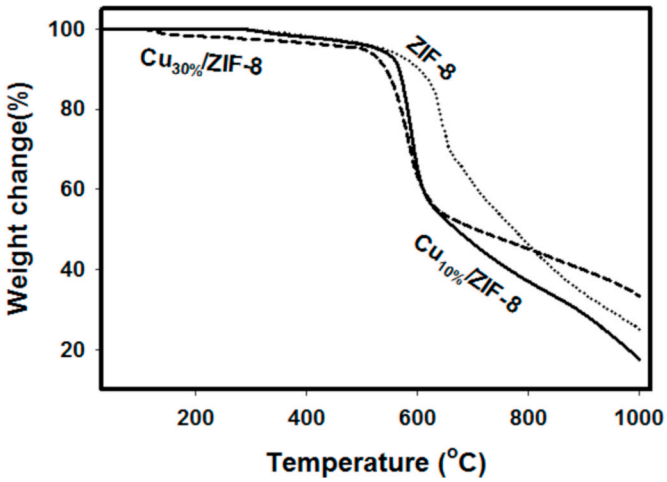

Fig. 7. TGA thermograms of ZIF-8, $Cu_{10\%}$/ZIF-8 and $Cu_{30\%}$/ZIF-8 samples in the range of 150 °C–1000 °C with heating rate 10 °C/min (Awadallah-F et al., 2019a).

corresponding to thermal stability of adsorbents studied by Awadallah et al. (Awadallah-F et al., 2019a) and Schejn et al. (2015) could be attributed to the differences in experimental conditions such as the respective synthesis methods. Moreover, the stability of ZIF-8 was improved by iron adding as Fe-ZIF-8(1:9) up to 250 °C and Fe-ZIF-8(2:8) up to 289 °C (Thanh et al., 2018). This phenomenon was also exhibited for TiO_2/ZIF-8 (Chandra et al., 2016).

3.5. Physical properties through gas adsorption

Using surface area and porosimetry analyzers that involve N_2 adsorption-desorption isotherm measurement at 77 K, along with possibly built-in density functional theory (DFT) calculations, is an effective characterization method that can provide details on the physical properties of ZIF-8 such as its surface area, micropore volume, total pore volume, and pore size distributions. The nitrogen adsorption-desorption isotherms of ZIF-8 show, generally, a type I isotherm as reported in several studies (Lai et al., 2016; Du et al., 2019; Zhang et al., 2019; Pan et al., 2011), representing a microporous structure. Fig. 8 (a) shows an example that represents this last behavior. Indeed, a microporous structure was confirmed by a rise in the adsorbed volume at very small relative pressures (Jian et al., 2015b).

Typical type-I isotherms were also obtained for samples ZIF-8, Zn/Co-ZIF-8, and Cu/ZIF-8 (Fig. 8 (b)), which indicates the presence of almost full microporosity (Awadallah-F et al., 2019d). However, behavior variation of isotherms to type-IV was achieved for P/P_0 values above 0.95. This could be attributed to the intra-aggregate voids that cause the presence of some large pores (Awadallah-F et al., 2019d).

The physical properties were affected by the synthesis conditions. For example, the specific surface areas presented in Table 1 changed with synthetic methods. Indeed, Jian et al. (2015a) have shown that the

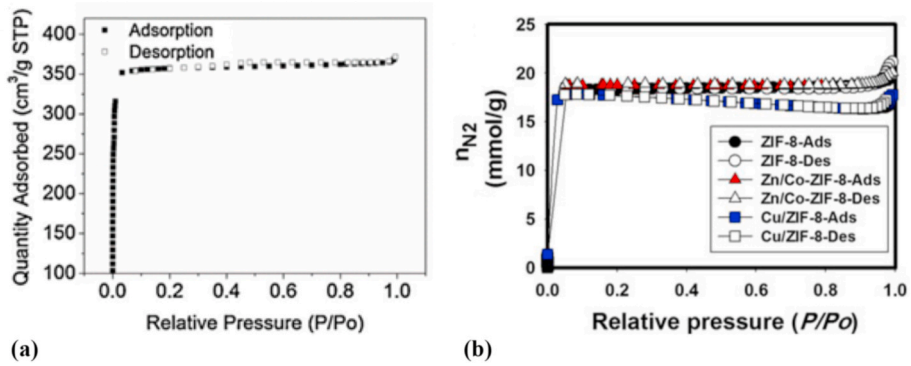

Fig. 8. (a) N_2 adsorption–desorption isotherms on ZIF-8 (Jian et al., 2015b), (b) N_2 adsorption–desorption onto ZIF-8, Zn/Co-ZIF-8, and Cu/ZIF-8 (Awadallah-F et al., 2019d).

reduction of the Hmim/Zn molar ratio from 70 to 10 leads to decreasing the BET surface area and the total pore volume of particles from 1126 m^2g^{-1} to 0.57 $cm^3\ g^{-1}$ to 31.9 m^2g^{-1} and 0.15 cm^3g^{-1}, respectively. This decrease was caused by the greater particle size distributions at little Hmim/Zn molar ratio. Khan et al. (2018) have confirmed that smaller particles have larger BET surface areas, higher micropore volumes, and larger external surface areas.

On the other hand, the effect of synthesis of ZIFs with pure or mixed metal and/or pure or mixed ligand on the physical properties has been reported in several studies (Awadallah-F et al., 2019b; Chen et al., 2018; Kaur et al., 2016; Botas et al., 2010; Caskey et al., 2008; Zhang et al., 2019; Liao et al., 2015). Synthesis of Cu^{2+}/ZIF-8 nanomaterials with various doping percentages (1%, 5%, 10% and 25%) was studied by Schejn et al. (2015). Indeed, the physical properties of pure ZIF-8 (S_{BET} = 1700 m^2g^{-1}, V_{micro} = 0.662cm^3g^{-1}) are shown to decrease only at a high doping percentage (25% of Cu^{2+}); whereas the pore size distribution is centered around 1.2 nm for all doping percentages of Cu, which agrees with that of the ZIF-8 (Jian et al., 2015a; Challa et al., 2011; Kida et al., 2013; Tanaka et al., 2012; Zhang et al., 2018; Binaeian et al., 2019; Xu et al., 2019; Schejn et al., 2015). Moreover, the decrease of both the specific surface area and pore volume when ZIF-8 is loaded with Ag/AgCl nanoparticles is probably associated to diverse catalytic extents of ZIF-8 as explained by Jing et al. (2020). Similarly, the ZIF-8 pore size did not change by Ag/AgCl loading since these nanoparticles were just inlaid in the body of ZIF-8 (Jing et al., 2020).

The temperature also has an effect onto the physical properties of ZIF-8 as described by Lai et al. (2016) for temperatures ranging from 80 °C to 140 °C. A successful synthesis of highly crystalline ZIF-8 was achieved at 120 °C with BET surface areas of up to 690.75 m^2g^{-1} and micropore volumes of up to 0.32 cm^3g^{-1}.

4. Potential applications of ZIF-8 materials and its derivatives

4.1. Separation of carbon dioxide (CO_2) gas

Effective CO_2 separation from other gases by adsorption or membranes is one of ZIF-8 advantages (Gong et al., 2017). Chi et al. (2015) investigated the CO_2/CH_4 separation using mixed matrix membranes (MMMs) generated from poly(styrene-block-ethylene-ranbutylene-bloc k-styrene) (SEBS) with different particle sizes of ZIF-8 and a fixed loading of 30 wt%. This is the ideal ZIF-8 concentration that leads to a good gas separation performance as reported in the literature (Chi et al., 2015; Zornoza et al., 2011). Indeed, the selectivity of CO_2/CH_4 separation is nearly independent of ZIF-8 particle sizes since the surface areas of particles remain constant; whereas the selectivity can be enhanced from 4.3 to 5.4 when adding ZIF-8 to the membrane (SEBS/ZIF-8 MMMS) compared to the neat polymer membrane (SEBS) (Chi et al., 2015). However, in a previous work (Zornoza et al., 2011) it is reported that ZIF-8 particle sizes could affect CO_2/CH_4 selectivity since ZIF-8 adsorbents have different surface areas with different sizes. Furthermore, a theoretical investigation of H_2 separation from CO_2 was presented by Bayati et al. (2019) using a ZIF-8 materials. The ZIF-8 nanomaterials exhibited a high tendency for CO_2 adsorption, while the diffusion coefficient of H_2 was much higher than that of CO_2. From a theoretical point of view, the obtained results prove that ZIF-8 has a H_2/CO_2 permselectivity greater than 30 at relatively low pressures (below 300 kPa), and it decreases at higher pressures. This result was interpreted by the progressive decrease of CO_2 adsorption contribution at lower pressures.

4.2. Separation of C_3 and C_4 hydrocarbons

ZIF-8 materials also exhibit excellent separation performances for hydrocarbons (Awadallah-F et al., 2019a; Yuan et al., 2017; Awadallah-F et al., 2019c; Pan et al., 2012). The high quality of ZIF-8 nanoparticles, functionalized by 5,6-dimethylbenzimidazole (DMBIM) through shell-ligand-exchange (SLE) reaction and integrated into polydimethylsiloxane (PDMS), prepared by Yuan et al. (2017) showed a significantly enhanced C_3H_8/N_2 separation performance in comparison with the pure PDMS membrane. Indeed, a C_3H_8 permeability over 2.10 $\times$ 10^4 Barrer and C_3H_8/N_2 selectivity of 99.5 were achieved. Another mixed matrix membrane fabricated by Zhang et al. (2012) via 6FDA--DAM polyimide and a ZIF-8 also showed a significantly enhanced propylene/propane (C_3H_6/C_3H_8) separation performance in comparison with the pure 6FDA-DAM membrane. The permeability and the ideal selectivity of C_3H_6 and C_3H_6/C_3H_8 of 56.2 Barrer and 31.0, respectively, were established when using ZIF-8 (48.0 wt%)/6FDA-DAM mixed matrix membrane. These values are, respectively, 258% and 150% greater than those obtained by the pure 6FDA-DAM membrane.

A novel approach was developed recently for the gas separation of isomers that are typically challenging to separate (e.g., propane vs. propylene and n-butane vs. isobutane) based on the concept of their distinguished threshold of nanogate-opening pressure (P_0). After this pressure threshold, long-chained molecules (e.g., C_3 and C_4 hydrocarbons) start to adsorb onto ZIFs as studied by Awadallah et al. (Awadallah-F et al., 2019a; Awadallah-F et al., 2019c). Indeed, ZIF-8 (Awadallah-F et al., 2019a; Awadallah-F et al., 2019c) and Cu/ZIF-8 (Awadallah-F et al., 2019a) and Co/ZIF-8 (Awadallah-F et al., 2019c) samples seem to widen the opening of their nanogates (meaning six-membered rings) at different threshold pressures during adsorption of diverse long-chain gases (such as propane, propylene, isobutane and *n*-butane) to a point that enables each of these molecules to be adsorbed (Awadallah-F et al., 2019a). Adsorption of such hydrocarbons will not occur at any pressures below this threshold. Consequently, P_0 has an important role in gas separation phenomenon on ZIFs where its value differs for each gas on the same ZIF. As a result, the separation of isomers

using ZIF-8 materials can be highly facilitated at intermediate pressure values between the P_0 values for the corresponding component. At such intermediate pressure (P), the component that has a P_0 value lower than P will be adsorbed, while that with a P_0 value higher than P will remain in the gas phase.

The values of P_0 were evaluated for each ZIF versus each gas by Awadallah et al. (Awadallah-F et al., 2019a) through fitting equilibrium adsorption data toward an empirical adsorption isotherm model that was modified from the Langmuir adsorption isotherm model to account for starting the adsorption process at such threshold pressures. On this basis, we seek in the next section to evaluate the P_0 value, with an understanding of framework responses and adsorption energetics against other theoretical adsorption isotherm models founded on a statistical physics approach, while respecting the author's permission (Awadallah-F et al., 2019a). Indeed, to the best of our knowledge, statistical physics theoretical approach was applied here for the first time on Zeolitic Imidazolate Framework (ZIF) membranes applications while attempting to consider the effect of nanogate opening pressures.

5. Correlation of adsorption data on ZIFs with nanogate opening pressures

An important number of investigations on ZIF-8 focused extensively on understanding how to correlate their experimental adsorption properties to theoretical methods such as molecular simulations (Krokidas et al., 2018), conventional molecular dynamics (Krokidas et al., 2017), DFT simulations (Hobday et al., 2018; Zheng et al., 2017), theoretical modeling (Awadallah-F et al., 2019a; Awadallah-F et al., 2019b; Awadallah-F et al., 2019c; Autie-Castro et al., 2017) … etc. The modeling of adsorption isotherms in gas or liquid phase adsorption is a powerful method for surface characterization (Al-Ghouti and Da'ana, 2020). Therefore, the fitting of experimental data by either theoretical or empirical models is necessary to investigate adsorption systems. Here, as an illustration, we present a combined experimental and computational approach to study the adsorption of small-to-medium sized molecules, especially of natural hydrocarbon gases by ZIF-8 (Awadallah-F et al., 2019a).

Table 4 shows theoretical models developed by our research group to account for the nanogate opening pressures for the adsorption of long-chained molecules on ZIFs. These models include the Modified Langmuir Model (MLM), Modified Ideal Monolayer Model (MIMM) and the Modified Real Monolayer Model (MRMM) presented in Equations (1)–(3), respectively. The last two models (MIMM and MRMM) are based on a statistical physics approach. Indeed, the statistical physics approach gives a physical meaning to the model's parameters and allows to describe phenomena outside the realm of traditional physics (Khalfaoui et al., 2003, 2015). The main advantage of the MRMM with respect to the MIMM is that it takes into account lateral interactions between adsorbed molecules (Khalfaoui et al., 2015) and thus describes a closer reality. These two theoretical models (MIMM and MRMM) will be compared to the semi-empirical one (MLM, Equation (1)). Indeed, P_0 in Equation (1) is a novel parameter presented into Langmuir model (Langmuir, 1916, 1918) by Awadallah et al. (Awadallah-F et al., 2019a; Awadallah-F et al., 2019c). This parameter is hypothetically introduced to represent the pressure threshold at which the ZIF crystal can adsorb the corresponding gas molecule where it is understood to widen its nanogate opening. According to this hypothesis, the same principle was applied to our two theoretical models (Equations (2) and (3)) by introducing the new parameter P_0.

The determination of the models' parameters is performed by nonlinear regression based on minimising the sum of squared errors, which corresponds to the least sum of squared errors (LSSE), between

Table 4
Theoretical adsorption models developed to account for nanogate opening pressures.

Theoretical models	Equations	Parameters	References
Modified Langmuir Model (MLM)	$Q_a(P)=\begin{cases}0 & , P \le P_0\\ m_L\dfrac{b_L(P-P_0)}{1+b_L(P-P_0)} & , P \ge P_0\end{cases}$ (1)	Q_a(mole /kg) is the adsorbed amount, P(Mpa) is the exposure pressure, m_L is the monolayer adsorption capacity, b_L is the adsorption affinity, P_0(Mpa) is the gate-opening pressure,	(Awadallah-F et al., 2019a)
Modified Ideal Monolayer Model (MIMM)	$Q_a(P)=\begin{cases}0 & , P \le P_0\\ \dfrac{n\times N_m}{1+\left(\dfrac{\alpha}{(P-P_0)}\right)^n} & , P \ge P_0\end{cases}$ (2)	n is the number of adsorbed molecule(s) per site, N_m is the receptor sites density(mol/kg), α is defined as: $\alpha = p_{1/2}-P_0$, where $p_{1/2}$ (MPa) is the half-saturation pressure,	Khalfaoui et al. (2003)
Modified Real Monolayer Model (MRMM)	$Q_a(P)=\begin{cases}0 & , P \le P_0\\ \dfrac{nN_m}{1+\left(w\dfrac{1-b(P-P_0)}{(P-P_0)}e^{2\beta a(P-P_0)}e^{-\dfrac{b(P-P_0)}{1-b(P-P_0)}}\right)^n} & , P \ge P_0\end{cases}$ (3)	b (MPa^{-1}) represents the covolume of the adsorbate molecule, a(J /MPa) is the corresponding molecular pressure cohesion, β is expressed as $(1/k_BT)$, where k_B is the Boltzmann's constant and T the experimental temperature, w is the characteristic concentration which was related to the energetic parameter as: $w = Z_{gtr}e^{-\beta\varepsilon} = p_{vs}e^{-\dfrac{\Delta E^a}{RT}}$ (4) where $p_{vs}(MPa)$ is the saturated vapor pressure, $R(J/K.mol)$ is the ideal gas constant, ΔE^a(kJ /mol) is the adsorption energy and Z_{gtr} is the translational partition function of an ideal gas molecule per volume unit,	Khalfaoui et al. (2015)

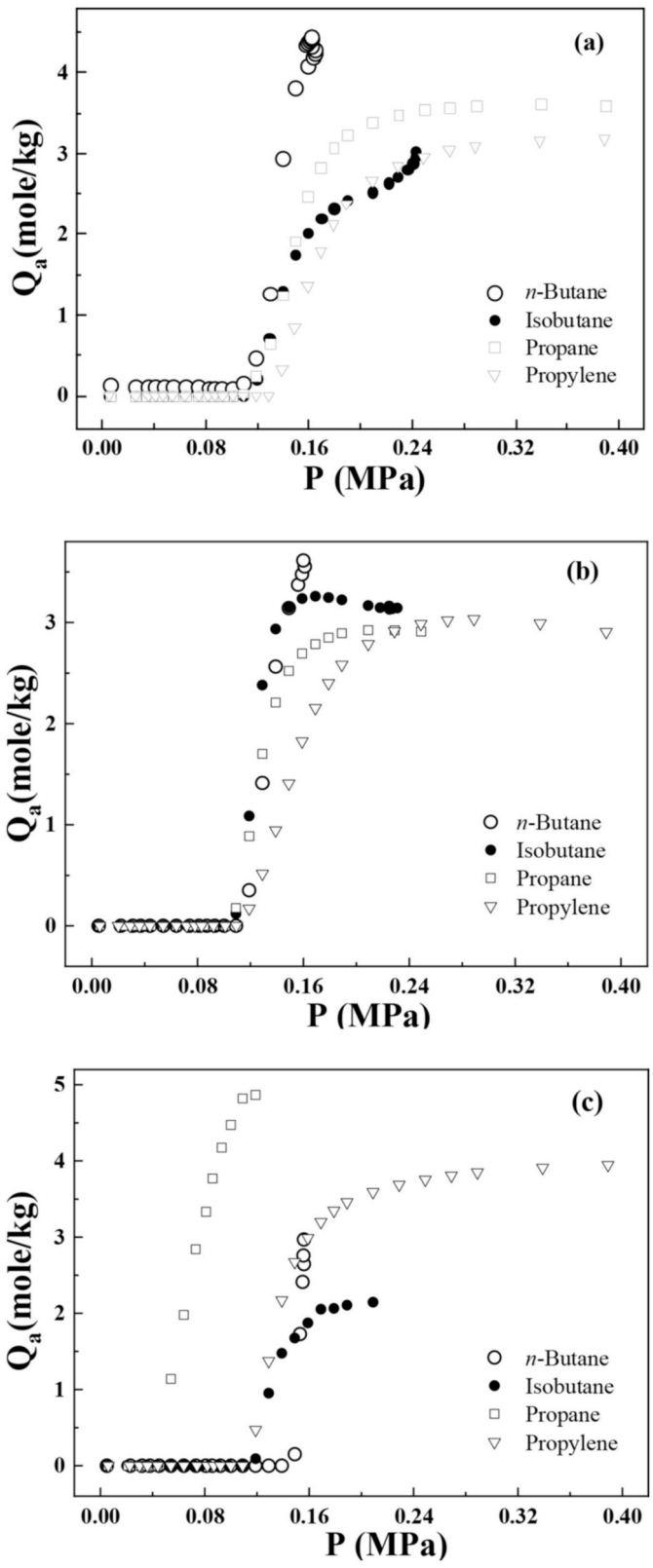

Fig. 9. Equilibrium adsorption isotherms of *n*-butane, isobutane, propane and propylene gases at 25 °C onto (a) ZIF-8, (b) $Cu_{10\%}$/ZIF-8 and (c) $Cu_{30\%}$/ZIF-8 (Awadallah-F et al., 2019a).

the experimental and correlated data using the Solver add-in of Microsoft Excel (Microsoft Corporation, 2016). The LSSE is defined by

$$\mathrm{LSSE} = \mathit{Minimum}\left[\sum_{i=1}^{j}(Q_{calc}-Q_{meas})_i^2\right] \quad (5)$$

where Q_{calc} is the correlated adsorbed amount (theoretical isotherm), Q_{meas} is the measured adsorbed amount, i is the data point number and j is the total number of data points. The corresponding errors were calculated based on the absolute relative error (ARE) (Kapoor and Yang, 1989):

$$\mathrm{ARE}\ (\%) = \frac{100}{j}\sum_{i=1}^{j}\left|\frac{Q_{calc}-Q_{meas}}{Q_{meas}}\right|_i \quad (6)$$

5.1. Experimental adsorption isotherms

Experimental adsorption isotherm data of *n*-butane, isobutane, propane, and propylene onto pure and Cu/ZIF-8 nanomaterials at 25 °C are presented in Fig. 9 (Awadallah-F et al., 2019a). It is observed from this figure that all gases exhibit no adsorption where the pressure increases up to an intermediate value that is specific for each gas on each adsorbent, which is defined by P_0. Indeed, when P is less than P_0, the opening nanogate of the ZIF crystal is considered to be insufficient for the free passage of molecules which hinders their adsorption, and thus the adsorbed quantity is zero. After this intermediate pressure, the behaviour of the adsorption isotherms exhibit a type-I behaviour according to the IUPAC classification (Awadallah-F et al., 2019a; Sing, 1985) where a plateau was reached. This behaviour was attributed to a surface saturation condition, which indicates that mesopores are filled as proved by Boudjema et al. (2020). The different aspects detected for *n*-butane, isobutane, propane, and propylene adsorption were attributed to the stereochemistry of each gas (Awadallah-F et al., 2019a).

It can be noticed from Fig. 9a that the sequential order in terms of equilibrium adsorption capacity onto ZIF-8 is *n*-butane > propane > isobutane ≈ propylene. For $Cu_{10\%}$/ZIF-8 adsorbent (Fig. 9b), this order becomes as *n*-butane > isobutane > propane > propylene. However, for $Cu_{30\%}$/ZIF-8 adsorbent (Fig. 9c), the order becomes propane > n-butane ≈ propylene > isobutane. Moreover, an increase of the adsorption rate of different gases was observed by Awadallah et al. (Awadallah-F et al., 2019a) following the increases of the concentration of Cu/ZIF-8 nanomaterials.

The values of nanogate opening pressures (P_0) for each gas is distinct on each adsorbent. Differences between P_0 values become more obvious for the Cu/ZIF-8, especially on $Cu_{30\%}$/ZIF-8. Consequently, coper-doped zeolitic imidazolate framework-8 showed an interesting tool for gas separation (Awadallah-F et al., 2019a; Goyal et al., 2018) based on the differences between the P_0 values of different components on the same adsorbent. For instance, if the operation pressure is set between the P_0 values of two components, the component with the lower P_0 value will be adsorbed whereas that with a higher P_0 value will not be adsorbed.

5.2. Theoretical fitting

All fitting parameters retrievable by MLM, MIMM and MRMM models are illustrated in Table 5. They are analyzed to investigate the adsorption systems more deeply. Hence, the best fitting model assessment was based firstly on minimizing SSE error function and then evaluated based on the magnitude of the ARE values. The lowest ARE values were obtained using the MRMM model (Table 5), leading to select it as the best fitting model.

Fig. 10 shows an example of experimental adsorption isotherm correlation of propylene onto $Cu_{10\%}$/ZIF-8 using the three adsorption isotherm models (Equations (1)–(3)). The best correlation between experimental isotherm and theoretical one is observed from MRMM. The better presentation of the MRMM model for experimental adsorption

Table 5
Fitting parameters of MLM, MIMM and MRMM models for the adsorption at 25 °C.

ZIF-8	Modified Langmuir Model (MLM)							
		m_L(mole/kg)		b_L(1/MP_a)	P_0(MP_a)		LSSE	ARE (%)
	n-Butane	5.485		90.395	0.125		0.789	3.1%
	Isobutane	3.621		31.278	0.120		0.130	2.5%
	Propane	4.373		29.955	0.123		0.658	6.3%
	Propylene	3.610		38.769	0.141		0.147	1.7%
	Modified Ideal Monolayer Model (MIMM)							
		n	N_m (mole/kg)	$P_{1/2}$(Mp_a)	P_0(Mp_a)		**LSSE**	**ARE (%)**
	n-Butane	0.443	29.203	0.284	0.127		0.608	2.6%
	Isobutane	0.596	12.022	0.347	0.118		0.177	6.9%
	Propane	0.279	27.205	0.355	0.138		0.869	4.9%
	Propylene	0.317	20.682	0.359	0.156		0.910	3.0%
	Modified Real Monolayer Model (MRMM)							
		n	N_m (mole/kg)	a (J/MP_a)	w (Mp_a)	b (1/Mp_a)	**P_0 (Mpa)**	**LSSE**	**ARE (%)**
	n-Butane	1.483	144.014	4.91E-20	0.212	0.105	0.120	0.531	**1.9%**
	Isobutane	1.140	272.062	5.31E-20	1.703	4.126	0.119	0.055	**0.7%**
	Propane	1.801	1.993	7.09E-23	0.044	3.197	0.111	0.026	**3.7%**
	Propylene	1.609	1.981	4.15E-22	0.039	1.738	0.129	0.002	**0.8%**
$Cu_{10\%}$/ZIF-8	Modified Langmuir Model (MLM)							
		m_L(mole/kg)		b_L(1/Mp_a)	P_0(Mp_a)		**LSSE**	**ARE (%)**
	n-Butane	5.018		64.279	0.122		0.132	**0.7%**
	Isobutane	3.316		303.801	0.117		0.170	3.0%
	Propane	3.337		79.824	0.114		0.090	2.3%
	Propylene	3.444		44.761	0.130		0.457	3.7%
	Modified Ideal Monolayer Model (MIMM)							
		n	N_m (mole/kg)	$P_{1/2}$(Mp_a)	P_0(Mp_a)		**LSSE**	**ARE (%)**
	n-Butane	0.466	21.983	0.258	0.126		0.131	**0.7%**
	Isobutane	0.129	51.792	0.315	0.118		0.328	4.0%
	Propane	0.304	21.555	0.296	0.118		0.213	4.3%
	Propylene	0.358	16.773	0.289	0.137		0.705	6.2%
	Modified Real Monolayer Model (MRMM)							
		n	N_m (mole/kg)	a (J/MP_a)	w (Mp_a)	b (1/Mp_a)	**P_0 (Mpa)**	**LSSE**	**ARE (%)**
	n-Butane	0.492	34.997	4.11E-20	0.398	5.019	0.125	0.131	**0.7%**
	Isobutane	0.543	49.994	6.56E-20	0.665	4.345	0.116	0.017	**0.4%**
	Propane	1.067	2.754	9.97E-22	0.013	7.066	0.113	0.041	**1.2%**
	Propylene	1.171	15.286	2.47E-20	0.180	1.684	0.119	0.047	**2.0%**
$Cu_{30\%}$/ZIF-8	Modified Langmuir Model (MLM)							
		m_L(mole/kg)		b_L(1/Mp_a)	P_0(Mp_a)		**LSSE**	**ARE (%)**
	n-Butane	4.688		290.472	0.151		0.094	3.9%
	Isobutane	2.482		83.207	0.121		0.018	**1.2%**
	Propane	9.016		17.625	0.046		0.109	3.5%
	Propylene	4.366		44.761	0.119		0.404	3.1%
	Modified Ideal Monolayer Model (MIMM)							
		n	N_m (mole/kg)	$P_{1/2}$(Mp_a)	P_0(Mp_a)		**LSSE**	**ARE (%)**
	n-Butane	0.985	60.001	0.301	0.148		0.061	2.9%
	Isobutane	0.354	14.476	0.297	0.125		0.034	2.6%
	Propane	0.906	11.969	0.128	0.046		0.132	**2.9%**
	Propylene	0.278	29.226	0.359	0.128		0.408	3.1%
	Modified Real Monolayer Model (MRMM)							
		n	N_m (mole/kg)	a (J/MP_a)	w (Mp_a)	b (1/Mp_a)	**P_0 (Mpa)**	**LSSE**	**ARE (%)**
	n-Butane	0.743	20.828	3.92E-21	0.089	30.288	0.148	0.061	**2.8%**
	Isobutane	0.996	2.510	1.13E-21	0.012	0.092	0.121	0.018	**1.2%**
	Propane	1.116	5.440	1.32E-21	0.041	4.306	0.044	0.083	**2.9%**
	Propylene	1.985	2.086	1.68E-20	0.024	1.576	0.110	0.002	0.5%

data exhibiting nanogate opening pressures can also be evidenced by its lower ARE values. Furthermore, the superiority of the MRMM model can be attributed to its ability to describe an intermediate adsorption process among the neighboring adsorbed molecules. Indeed, adsorbed molecules can establish attraction or repulsion force with the neighboring molecules, subsequently, adsorbate-adsorbate interactions cannot be neglected (Khalfaoui et al., 2015). Hence, the adsorbent surface chemistry plays an important role in the interactions kind involved in the adsorption process (Lin et al., 2015; Nakhli et al., 2020). As a result, in the next paragraph, we try to interpret some parameters related to the MRMM fitting of the studied systems.

Fig. 11 shows the evolutions of w and b parameters with P_0 of n-butane, isobutane, propane and propylene gases onto ZIF-8 and Cu/ZIF-8. Indeed, w is the characteristic concentration that varies inversely with the energetic parameter as presented by Equation (4) (Table 4), and b represents the covolume of the adsorbate molecule. It can be noticed that the same evolution behavior has been detected for both w and b parameters with P_0. Moreover, the same evolution was also detected following the values of w and molecular pressure cohesion (a) parameters with P_0 (Table 5). Consequently, it can be concluded that the higher covolume of adsorbate molecule and the higher molecular pressure cohesion led to the lower adsorption energy. Indeed, the change of parameters b and a could be attributed to the stereochemistry of each gas (Awadallah-F et al., 2019a) that affect the adsorption energy.

The adsorption energy is an important parameter that leads to a better understanding of the results obtained by Awadallah et al.

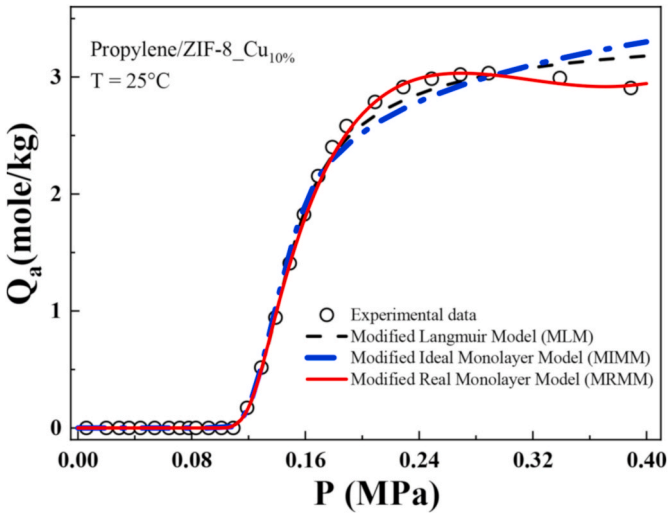

Fig. 10. Fitting of isotherm data for the adsorption of propylene onto $Cu_{10\%}$/ZIF-8 adsorbent at 25 °C using the three adsorption isotherm models (MLM, MIMM and MRMM).

(Awadallah-F et al., 2019a). These authors have shown the importance of P_0 parameter in relation with gas separation performances. Indeed, P_0 values were found to be the same for both *n*-butane and isobutane couple in the case of ZIF-8 adsorbent since they have the same chemical formula (C_4H_{10}), and hence the stereochemistry of each gas can explain the difference in adsorption capacity (Awadallah-F et al., 2019a). Indeed, *n*-butane molecule can easy penetrate the nanogate with less difficulty compared to the branched isobutane molecule (Awadallah-F et al., 2019a) and this is due to the linearity of the first one. Then, there is a difficulty to separate these molecules on ZIF-8 due to the approaching values of P_0. The same reflection was observed for propane and propylene in the case of ZIF-8 adsorbent (Awadallah-F et al., 2019a). Thereafter, the P_0 values were changed for each couple following the increases of Cu/ZIF-8 percentage. Therefore, it was concluded that $Cu_{30\%}$/ZIF-8 adsorbent is more adequate than $Cu_{10\%}$/ZIF-8 and ZIF-8 adsorbents for gases separation on the basis of differences between their P_0 values (Awadallah-F et al., 2019a). As a result, the conclusion about adsorption energy parameter deduced from *w* supports well these results. Indeed, as presented in Table 6, the variations of adsorption energy (estimated from Δw) and of P_0 increase follow the increase of Cu/ZIF-8 percentage for each couple of *n*-butane/isobutene and propane/propylene. Then, it can be deduced that the increase of copper percentage doped in ZIF-8 affects as well the adsorption energy, and then the variation of P_0 values for each pair of isomers. Consequently, the importance of P_0 parameter in relation with gas separation performances detected by Awadallah et al. (Awadallah-F et al., 2019a) could be related to the importance of the adsorption energy for each gas following the increase of copper percentage doped into ZIF-8. On the other hand, the difference in adsorption capacity from one gas to another by changing the copper percentage doped in ZIF-8 does not follow the same order. This point was attributed to several factors, as the stereochemistry and the polarity of each gas.

6. Conclusions

This review focuses on the latest synthesis methods of ZIF-8 and its derivatives; in addition to their common characterization techniques and their corresponding applications. Light was shed on the potential application of ZIF-8 in gas separation and the theoretical modeling of their adsorption isotherms was discussed. A statistical physics approach was applied in this review to correlate the experimental adsorption isotherms of some gases by ZIF-8 and its derivatives. As a state of the art,

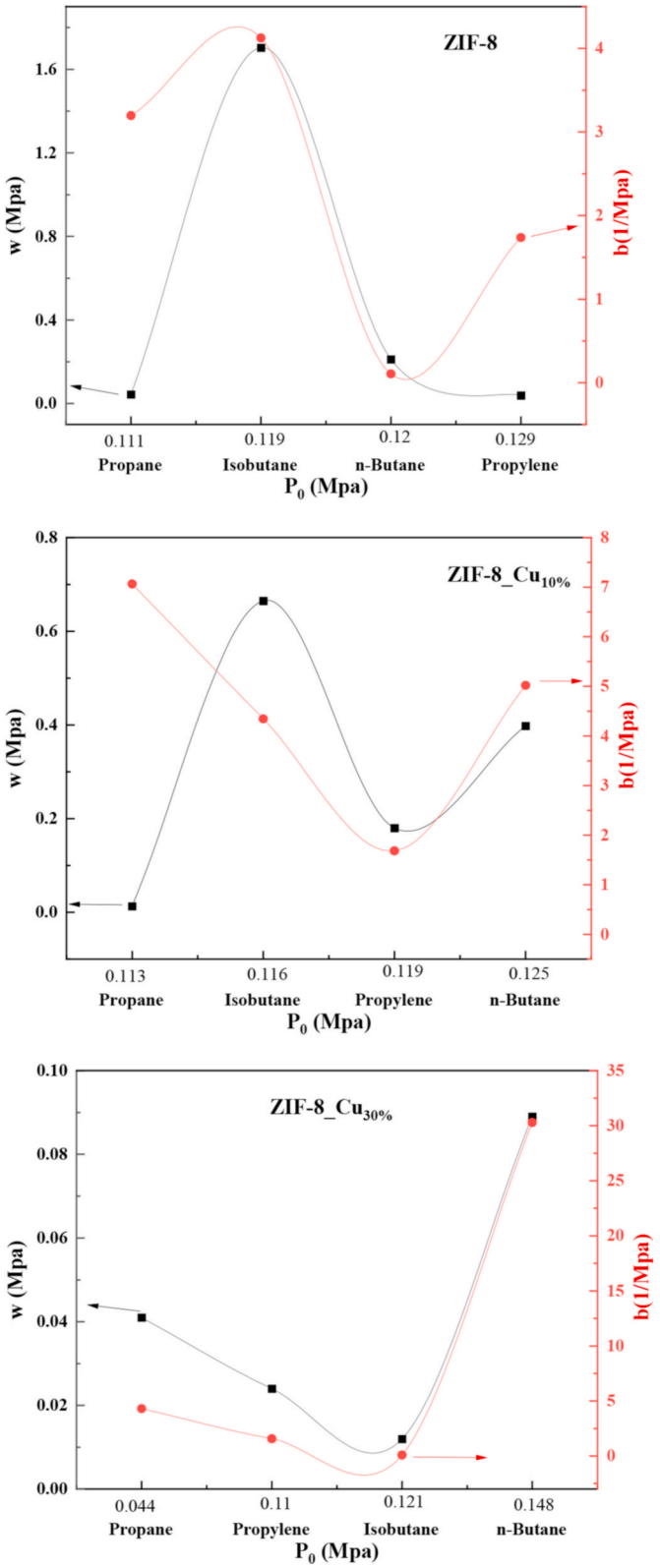

Fig. 11. Evolutions of *w* and *b* parameters with P_0 values for each gas with different Cu/ZIF-8 percentages.

we treated the case of *n*-butane, isobutane, propane and propylene gases separations using ZIF-8 and Cu/ZIF-8 nanomaterials (Awadallah-F et al., 2019a). Some specific properties such as "gate opening" mechanism, is systematically described and discussed based on the statistical physics approach.

Table 6
Values of P_0, ΔP_0, w and Δw fitting parameters for the isomer pairs of n-butane/isobutane and propane/propylene as calculated from MRMM model at 25 °C.

		P_0 (MPa)	ΔP_0 (MPa)	w (MPa)	Δw (MPa)
ZIF-8	n-Butane	0.120	0.001	0.212	1.491
	Isobutane	0.119		1.703	
$Cu_{10\%}$/ZIF-8	n-Butane	0.125	0.009	0.398	0.267
	Isobutane	0.116		0.665	
$Cu_{30\%}$/ZIF-8	n-Butane	0.148	0.027	0.089	0.077
	Isobutane	0.121		0.012	
ZIF-8	Propane	0.111	0.018	0.044	0.005
	Propylene	0.129		0.039	
$Cu_{10\%}$/ZIF-8	Propane	0.113	0.006	0.013	0.167
	Propylene	0.119		0.180	
$Cu_{30\%}$/ZIF-8	Propane	0.044	0.066	0.041	0.017
	Propylene	0.110		0.024	

As main conclusions, by increasing the Cu/ZIF-8 percentage, the values of the gate opening pressure (P_0) were changed for each isomer pair of n-butane/isobutane and propane/propylene, which enhances the performances of gas separation at pressures between their corresponding P_0 values. Consequently, $Cu_{30\%}$/ZIF-8 adsorbent is more suitable than $Cu_{10\%}$/ZIF-8 and ZIF-8 adsorbents for gas separations thanks to the exhibited differences in P_0 values. This point was confirmed by the adsorption energy parameter derived from statistical physics approach. Indeed, the importance of gate opening pressure could be related to the importance of the adsorption energy for each gas following the increases of Cu/ZIF-8 percentage. From this, we can infer that the specific characteristics of ZIF-8 and its derivatives will allow for various important applications ranging from sensing and electronic devices to drug delivery, and therefore offers a promising research field to be explored. In view of the great interest of several research groups, new concepts and techniques for the synthesis of ZIF are being adopted. In addition, the rapid growth of new applications and new opportunities for further exploration of ZIF materials will continue to emerge in the future. In fact, due to the lack of functional groups in natural ZIF8 particles, they are not suitable for many applications. For this, functional groups were necessary through the use of, e.g., amino reactive imidazole derivatives and doped ZIFs materials. Moreover, computational methods are important nowadays to complement experimental measurements.

Availability of data and material

All data generated or analyzed during this study are included in this article.

Funding

Not applicable.

Author contributions

Manel Bergaoui: Conceptualization, Investigation, Work Execution, Methodology, Software, Writing- original draft. Ahmed Awadallah-F: Conceptualization, Investigation, Work Execution, Methodology, Software, Writing- original draft. Mohamed Khalfaoui: Conceptualization, Investigation, Methodology, Supervision, Validation, Writing - reviewing and editing. Shaheen A. Al-Muhtaseb: Conceptualization, Investigation, Methodology, Supervision, Validation, Writing - reviewing and editing.

Declaration of competing interest

The authors declare that they have no known competing financial interests or personal relationships that could have appeared to influence the work reported in this paper.

Acknowledgements

Open Access funding provided by the Qatar National Library.

References

Aboraia, A.M., Darwish, A.A.A., Polyakov, V., Erofeeva, E., Butova, V., Zahran, H.Y., El-Rehim, A.F.A., Algarni, H., Yahia, I.S., Soldatov, A.V., 2020. Structural characterization and optical properties of zeolitic imidazolate frameworks (ZIF-8) for solid-state electronics applications. Opt. Mater. 100, 109648.
Al-Ghouti, M.A., Da'ana, D.A., 2020. Guidelines for the use and interpretation of adsorption isotherm models: a review. J. Hazard Mater. 393, 122383.
Autie-Castro, G., Oliveira, D., Autié Castro, G., Jardim, E.d.O., Reguera, E., Vilarrasa-García, E., Rodríguez-Castellón, E., Cavalcante Jr., C.L., 2017. CH_4 and CO_2 adsorption study in ZIF-8 and Al-BDC MOFs. Bio. Chem. Res. 4, 234–246.
Awadallah-F, A., Hillman, F., Al-Muhtaseb, S.A., Jeong, H.-K., 2019a. On the nanogate-opening pressures of copper-doped zeolitic imidazolate framework ZIF-8 for the adsorption of propane, propylene, isobutane, and n-butane. J. Mater. Sci. 54, 5513–5527.
Awadallah-F, A., Hillman, F., Al-Muhtaseb, S.A., Jeong, H.-K., 2019b. Adsorption of carbon dioxide, methane, and nitrogen gases onto ZIF compounds with zinc, cobalt, and zinc/cobalt metal centers. J. Nanomater. 2019, 1–11.
Awadallah-F, A., Hillman, F., Al-Muhtaseb, S.A., Jeong, H.-K., 2019c. Nano-gate opening pressures for the adsorption of isobutane, n-butane, propane, and propylene gases on bimetallic Co–Zn based zeolitic imidazolate frameworks. Dalton Trans. 48, 4685–4695.
Awadallah-F, A., Hillman, F., Al-Muhtaseb, S.A., Jeong, H.-K., 2019d. Influence of doped metal center on morphology and pore structure of ZIF-8. MRS Commun 9, 288–291.
Banerjee, R., Phan, A., Wang, B., Knobler, C., Furukawa, H., O'Keeffe, M., Yaghi, O.M., 2008. High-throughput synthesis of zeolitic imidazolate frameworks and application to CO2 capture. Sci 319, 939–943.
Bao, Q., Lou, Y., Xing, T., Chen, J., 2013. Rapid synthesis of zeolitic imidazolate framework-8 (ZIF-8) in aqueous solution via microwave irradiation. Inorg. Chem. Commun. 37, 170–173.
Bayati, B., Ghorbani, A., Ghasemzadeh, K., Iulianelli, A., Basile, A., 2019. Study on the separation of H_2 from CO_2 using a ZIF-8 membrane by molecular simulation and maxwell-stefan model. Mol 24, 4350.
Bernardo, P., Drioli, E., Golemme, G., 2009. Membrane gas separation: a review/state of the art. Ind. Eng. Chem. Res. 48, 4638–4663.
Binaeian, E., Maleki, S., Motaghedi, N., Arjmandi, M., 2019. Study on the performance of Cd2+ sorption using dimethylethylenediamine-modified zinc-based MOF (ZIF-8-mmen): optimization of the process by RSM technique. Separ. Sci. Technol. 55, 1–16.
Biswal, B.P., Shinde, D.B., Pillai, V.K., Banerjee, R., 2013. Stabilization of graphene quantum dots (GQDs) by encapsulation inside zeolitic imidazolate framework nanocrystals for photoluminescence tuning. Nanoscale 5, 10556–10561.
Botas, J.A., Calleja, G., Sánchez-Sánchez, M., Orcajo, M.G., 2010. Cobalt doping of the MOF-5 framework and its effect on gas-adsorption properties. Langmuir 26, 5300–5303.
Boudjema, L., Long, J., Petitjean, H., Larionova, J., Guari, Y., Trens, P., Salles, F.J.I.C.A., 2020. Adsorption of volatile organic compounds by ZIF-8, Cu-BTC and a Prussian blue analogue. A comparative study 501, 119316.
Caskey, S.R., Wong-Foy, A.G., Matzger, A.J., 2008. Dramatic tuning of carbon dioxide uptake via metal substitution in a coordination polymer with cylindrical pores. J. Am. Chem. Soc. 130, 10870–10871.
Challa, S.R., Delariva, A.T., Hansen, T.W., Helveg, S., Sehested, J., Hansen, P.L., Garzon, F., Datye, A.K., 2011. Relating rates of catalyst sintering to the disappearance of individual nanoparticles during Ostwald ripening. J. Am. Chem. Soc. 133, 20672–20675.
Chandra, R., Mukhopadhyay, S., Nath, M., 2016. TiO_2@ ZIF-8: a novel approach of modifying micro-environment for enhanced photo-catalytic dye degradation and high usability of TiO_2 nanoparticles. Mater. Lett. 164, 571–574.
Chen, H., Wang, J., 2020. MOF-derived Co3O4-C@ FeOOH as an efficient catalyst for catalytic ozonation of norfloxacin. J. Hazard Mater. 403, 123697.
Chen, B., Yang, Z., Zhu, Y., Xia, 2014. Zeolitic imidazolate framework materials: recent progress in synthesis and applications, 2, 16811–16831. Y.J.J.o.M.C.A.
Chen, G., Yu, B., Lu, C., Zhang, H., Shen, Y., Cong, H., 2018. Controlled synthesis of Fe3O4@ ZIF-8 nanoparticles for drug delivery. CrystEngComm 20, 7486–7491.
Chen, X., Jiang, X., Yin, C., Zhang, B., Zhang, Q., 2019. Facile fabrication of hierarchical porous ZIF-8 for enhanced adsorption of antibiotics. J. Hazard Mater. 367, 194–204.
Chi, W.S., Hwang, S., Lee, S.-J., Park, S., Bae, Y.-S., Ryu, D.Y., Kim, J.H., Kim, J., 2015. Mixed matrix membranes consisting of SEBS block copolymers and size-controlled ZIF-8 nanoparticles for CO_2 capture. J. Membr. Sci. 495, 479–488.
Chin, M., Cisneros, C., Araiza, S.M., Vargas, K.M., Ishihara, K.M., Tian, F., 2018. Rhodamine B degradation by nanosized zeolitic imidazolate framework-8 (ZIF-8). RSC Adv. 8, 26987–26997.
Cho, H., Kim, J., Kim, S.-N., Ahn, W.-s., 2013. High yield 1-L scale synthesis of ZIF-8 via a sonochemical route. Microporous Mesoporous Mater. 169, 180–184.
Du, P.D., Thanh, D., Viet, N., Hieu, N.T., 2019. Evaluation of structural properties and catalytic activities in knoevenagel condensation reaction of zeolitic imidazolate framework-8 synthesized under different conditions. Adv. Mater. Sci. Eng. 2019, 1–8.
Duan, H., Hu, X., Sun, Z., 2020. Magnetic zeolite imidazole framework material-8 as an effective and recyclable adsorbent for removal of ceftazidime from aqueous solution. J. Hazard Mater. 384, 121406.

Dunne, P.W., Munn, A.S., Starkey, C.L., Huddle, T.A., Lester, E.H., 2015. Continuous-flow hydrothermal synthesis for the production of inorganic nanomaterials. Phil. Trans. Math. Phys. Eng. Sci. 373, 20150015.
Fang, C., Cen, D., Wang, Y., Wu, Y., Cai, X., Li, X., Han, G., 2020. ZnS@ ZIF-8 core-shell nanoparticles incorporated with ICG and TPZ to enable H_2S-amplified synergistic therapy. Theranostics 10, 7671–7682.
Feng, S., Zhang, X., Shi, D., Wang, 2021. Engineering, Zeolitic imidazolate framework-8 (ZIF-8) for drug delivery: a critical review, 15, 221–237. Z.J.F.o.C.S.
Fu, F., Zheng, B., Xie, L.-H., Du, H., Du, S., Dong, Z., 2018. Size-controllable synthesis of zeolitic imidazolate framework/carbon nanotube composites. Crystals 8, 367.
Gong, X., Wang, Y., Kuang, T., 2017. ZIF-8-based membranes for carbon dioxide capture and separation. ACS Sustain. Chem. Eng. 5, 11204–11214.
Goyal, S., Shaharun, M.S., Kait, C.F., Abdullah, B., 2018. Effect of monometallic copper on zeolitic imidazolate framework-8 synthesized by hydrothermal method. J. Phys. Conf. Ser. 1123, 12062.
Hobday, C.L., Woodall, C.H., Lennox, M.J., Frost, M., Kamenev, K., Düren, T., Morrison, C.A., Moggach, S.A., 2018. Understanding the adsorption process in ZIF-8 using high pressure crystallography and computational modelling. Nat. Commun. 9, 1–9.
Howarth, A.J., Liu, Y., Li, P., Li, Z., Wang, T.C., Hupp, J.T., Farha, O.K., 2016. Chemical, thermal and mechanical stabilities of metal–organic frameworks. Nat. Rev. Mater. 1, 1–15.
Huang, X.C., Lin, Y.Y., Zhang, J.P., Chen, X.M., 2006. Ligand-directed strategy for zeolite-type metal–organic frameworks: zinc (II) imidazolates with unusual zeolitic topologies. Angew. Chem. Int. Ed. 45, 1557–1559.
Jian, M., Liu, B., Liu, R., Qu, J., Wang, H., Zhang, X., 2015a. Water-based synthesis of zeolitic imidazolate framework-8 with high morphology level at room temperature. RSC Adv. 5, 48433–48441.
Jian, M., Liu, B., Zhang, G., Liu, R., Zhang, X., 2015b. Adsorptive removal of arsenic from aqueous solution by zeolitic imidazolate framework-8 (ZIF-8) nanoparticles. Colloids Surf., A 465, 67–76.
Jing, Y., Lei, Q., Xia, C., Guan, Y., Yang, Y., He, J., Yang, Y., Zhang, Y., Yan, M., 2020. Synthesis of Ag and AgCl co-doped ZIF-8 hybrid photocatalysts with enhanced photocatalytic activity through a synergistic effect. RSC Adv. 10, 698–704.
Kapoor, A., Yang, R., 1989. Correlation of equilibrium adsorption data of condensible vapours on porous adsorbents. Gas Separ. Purif. 3, 187–192.
Kaur, G., Rai, R.K., Tyagi, D., Yao, X., Li, P.-Z., Yang, X.-C., Zhao, Y., Xu, Q., Singh, S.K., 2016. Room-temperature synthesis of bimetallic Co–Zn based zeolitic imidazolate frameworks in water for enhanced CO_2 and H_2 uptakes. J. Mater. Chem. 4, 14932–14938.
Khalfaoui, M., Knani, S., Hachicha, M., Ben Lamine, A., 2003. New theoretical expressions for the five adsorption type isotherms classified by BET based on statistical physics treatment. J. Colloid Interface Sci. 263, 350–356.
Khalfaoui, M., El Ghali, A., Aguir, C., Mohamed, Z., Baouab, M.H.V., Ben Lamine, A., 2015. Study on adsorption of herbicide onto functionalized cellulose extracted from Juncusacutus L. plant: experimental results and theoretical modeling. Ind. Crop. Prod. 67, 169–178.
Khan, I.U., Othman, M.H.D., Jilani, A., Ismail, A., Hashim, H., Jaafar, J., Rahman, M.A., Rehman, G.U., 2018. Economical, environmental friendly synthesis, characterization for the production of zeolitic imidazolate framework-8 (ZIF-8) nanoparticles with enhanced CO_2 adsorption. Arabian J. Chem. 11, 1072–1083.
Kida, K., Okita, M., Fujita, K., Tanaka, S., Miyake, Y., 2013. Formation of high crystalline ZIF-8 in an aqueous solution. CrystEngComm 15, 1794–1801.
Krokidas, P., Castier, M., Economou, I.G., 2017. Computational study of ZIF-8 and ZIF-67 performance for separation of gas mixtures. J. Phys. Chem. C 121, 17999–18011.
Krokidas, P., Moncho, S., Brothers, E.N., Castier, M., Economou, I.G., 2018. Tailoring the gas separation efficiency of metal organic framework ZIF-8 through metal substitution: a computational study. Phys. Chem. Chem. Phys. 20, 4879–4892.
Lai, L.S., Yeong, Y.F., Lau, K.K., Shariff, A.M., 2016. Effect of synthesis parameters on the formation of ZIF-8 under microwave-assisted solvothermal. Procedia Eng 148, 35–42.
Langmuir, I., 1916. The constitution and fundamental properties of solids and liquids. Part I. Solids. J. Am. Chem. Soc. 38, 2221–2295.
Langmuir, I., 1918. The adsorption of gases on plane surfaces of glass, mica and platinum. J. Am. Chem. Soc. 40, 1361–1403.
Lee, Y.-R., Jang, M.-S., Cho, H.-Y., Kwon, H.-J., Kim, S., Ahn, W.-S., 2015. ZIF-8: a comparison of synthesis methods. Chem. Eng. J. 271, 276–280.
Li, N., Zhou, L., Jin, X., Owens, G., Chen, Z., 2019. Simultaneous removal of tetracycline and oxytetracycline antibiotics from wastewater using a ZIF-8 metal organic-framework. J. Hazard Mater. 366, 563–572.
Li, J., Chang, H., Li, Y., Li, Q., Shen, K., Yi, H., Zhang, J., 2020. Synthesis and adsorption performance of La@ZIF-8 composite metal–organic frameworks. RSC Adv. 10, 3380–3390.
Li, K., Miwornunyuie, N., Chen, L., Jingyu, H., Amaniampong, P.S., Ato Koomson, D., Ewusi-Mensah, D., Xue, W., Li, G., Lu, H.J.S., 2021. Sustainable application of ZIF-8 for heavy-metal removal in aqueous solutions, 13, 984.
Liao, Y.-T., Dutta, S., Chien, C.-H., Hu, C.-C., Shieh, F.-K., Lin, C.-H., Wu, K.C.-W., 2015. Synthesis of mixed-ligand zeolitic imidazolate framework (ZIF-8-90) for CO_2 adsorption. J. Inorg. Organomet. Polym. Mater. 25, 251–258.
Lin, Y.-H., Jeng, H.-T., Lin, D.-S., 2015. Separation of the attractive and repulsive contributions to the adsorbate–adsorbate interactions of polar adsorbates on Si(100). Surf. Sci. 641, 282–288.
Liu, J., He, J., Wang, L., Li, R., Chen, P., Rao, X., Deng, L., Rong, L., Lei, J., 2016. NiO-PTA supported on ZIF-8 as a highly effective catalyst for hydrocracking of Jatropha oil. Sci. Rep. 6, 23667.
Liu, F., Xiong, W., Feng, X., Shi, L., Chen, D., Zhang, Y., 2019. A novel monolith ZnS-ZIF-8 adsorption material for ultraeffective Hg (II) capture from wastewater. J. Hazard Mater. 367, 381–389.
Lu, S., Hummel, M., Chen, K., Zhou, Y., Kang, S., Gu, Z., 2020. Synthesis of Au@ ZIF-8 nanocomposites for enhanced electrochemical detection of dopamine. Electrochem. Commun. 114, 106715.
Lucero, J., Osuna, C., Crawford, J.M., Carreon, M.A., 2019. Microwave-assisted synthesis of porous organic cages CC3 and CC2. CrystEngComm 21, 4534–4537.
Ma, X., Liu, D., 2019. Zeolitic imidazolate framework membranes for light olefin/paraffin separation. Crystals 9, 14.
Mahmoodi, N.M., Oveisi, M., Taghizadeh, A., Taghizadeh, M., 2019. Novel magnetic amine functionalized carbon nanotube/metal-organic framework nanocomposites: from green ultrasound-assisted synthesis to detailed selective pollutant removal modelling from binary systems. J. Hazard Mater. 368, 746–759.
Martinez Joaristi, A., Juan-Alcañiz, J., Serra-Crespo, P., Kapteijn, F., Gascon, J., 2012. Electrochemical synthesis of some archetypical Zn^{2+}, Cu^{2+}, and Al^{3+} metal organic frameworks. Cryst. Growth Des. 12, 3489–3498.
Matsuoka, A., Matsumura, H., Odaka, M., Ogawa, N., Tanno, T., 2018. The transitional transmittance response of ZIF-8 gas adsorption observed using terahertz waves. e-J. Surf. Sci. Nanotechnol. 16, 142–144.
Melgar, V.M.A., Kim, J., Othman, M.R., 2015. Zeolitic imidazolate framework membranes for gas separation: a review of synthesis methods and gas separation performance. J. Ind. Eng. Chem. 28, 1–15.
Muñoz-Gil, D., Figueiredo, F.M., 2019. High surface proton conduction in nanostructured ZIF-8. Nanomaterials 9, 1369.
Nakhli, A., Bergaoui, M., Toumi, K.H., Khalfaoui, M., Benguerba, Y., Balsamo, M., Soetaredjo, F.E., Ismadji, S., Ernst, B., Erto, A., 2020. Molecular insights through computational modeling of methylene blue adsorption onto low-cost adsorbents derived from natural materials: a multi-model's approach. Comput. Chem. Eng. 140, 106965.
Neelakanda, P., Barankova, E., Peinemann, K.-V., 2016. Polymer supported ZIF-8 membranes by conversion of sputtered zinc oxide layers. Microporous Mesoporous Mater. 220, 215–219.
Pan, Y., Liu, Y., Zeng, G., Zhao, L., Lai, Z., 2011. Rapid synthesis of zeolitic imidazolate framework-8 (ZIF-8) nanocrystals in an aqueous system. Chem. Commun. 47, 2071–2073.
Pan, Y., Li, T., Lestari, G., Lai, Z., 2012. Effective separation of propylene/propane binary mixtures by ZIF-8 membranes. J. Membr. Sci. 390– 391, 93–98.
Park, K.S., Ni, Z., Côté, A.P., Choi, J.Y., Huang, R., Uribe-Romo, F.J., Chae, H.K., O'Keeffe, M., Yaghi, O.M., 2006. Exceptional chemical and thermal stability of zeolitic imidazolate frameworks. Proc. Natl. Acad. Sci. U.S.A. 103, 10186–10191.
Payra, S., Reddy, K.L., Sharma, R.S., Singh, S., Roy, S., 2020. A trade-off between adsorption and photocatalysis over ZIF-derived composite. J. Hazard Mater. 393, 122491.
Pillai, P., Dharaskar, S., Sasikumar, S., Khalid, M., 2019. Zeolitic imidazolate framework-8 nanoparticle: a promising adsorbent for effective fluoride removal from aqueous solution. Appl. Water Sci. 9, 150.
Pullumbi, P., Brandani, F., Brandani, S., 2019. Gas separation by adsorption: technological drivers and opportunities for improvement. Curr. Opin. Chem. Eng. 24, 131–142.
Radhakrishnan, D., Narayana, C., 2016. Guest dependent Brillouin and Raman scattering studies of zeolitic imidazolate framework-8 (ZIF-8) under external pressure. J. Chem. Phys. 144, 134704.
Rubio-Martinez, M., Avci-Camur, C., Thornton, A.W., Imaz, I., Maspoch, D., Hill, M.R., 2017. New synthetic routes towards MOF production at scale. Chem. Soc. Rev. 46, 3453–3480.
Samadi-Maybodi, A., Ghasemi, S., Ghaffari-Rad, H., 2015. A novel sensor based on Ag-loaded zeolitic imidazolate framework-8 nanocrystals for efficient electrocatalytic oxidation and trace level detection of hydrazine. Sens. Actuators, B 220, 627–633.
Sankar, S.S., Karthick, K., Sangeetha, K., Karmakar, A., Kundu, S., 2019. Transition-metal-based zeolite imidazolate framework nanofibers via an electrospinning approach: a review. ACS Omega 5, 57–67.
Schejn, A., Balan, L., Falk, V., Aranda, L., Medjahdi, G., Schneider, R., 2014. Controlling ZIF-8 nano-and microcrystal formation and reactivity through zinc salt variations. CrystEngComm 16, 4493–4500.
Schejn, A., Aboulaich, A., Balan, L., Falk, V., Lalevée, J., Medjahdi, G., Aranda, L., Mozet, K., Schneider, R., 2015. Cu 2+-doped zeolitic imidazolate frameworks (ZIF-8): efficient and stable catalysts for cycloadditions and condensation reactions. Catal. Sci. Technol. 5, 1829–1839.
Shi, Q., Chen, Z., Song, Z., Li, J., Dong, J., 2011. Synthesis of ZIF-8 and ZIF-67 by steam-assisted conversion and an investigation of their tribological behaviors. Angew. Chem. Int. Ed. 50, 672–675.
Sing, K.S., 1985. Reporting physisorption data for gas/solid systems with special reference to the determination of surface area and porosity (Recommendations 1984). Pure Appl. Chem. 57, 603–619.
Song, Q., Nataraj, S., Roussenova, M.V., Tan, J.C., Hughes, D.J., Li, W., Bourgoin, P., Alam, M.A., Cheetham, A.K., Al-Muhtaseb, S.A., 2012. Zeolitic imidazolate framework (ZIF-8) based polymer nanocomposite membranes for gas separation. Energy Environ. Sci. 5, 8359–8369.
Sze Lai, L., Fong Yeong, Y., Keong Lau, K., Shariff Az, M., 2014a. Zeolite imidazole frameworks membranes for CO_2/CH_4 separation from natural gas: a review. J. Appl. Sci. 14, 1161–1167.
Sze Lai, L., Fong Yeong, Y., Keong Lau, K., Shariff Az, 2014b. Zeolite imidazole frameworks membranes for CO2/CH4 separation from natural gas. A review 14, 1161–1167. M.J.J.o.A.S.

Tanaka, S., Kida, K., Okita, M., Ito, Y., Miyake, Y., 2012. Size-controlled synthesis of zeolitic imidazolate framework-8 (ZIF-8) crystals in an aqueous system at room temperature. Chem. Lett. 41, 1337–1339.

Tanaka, S., Fujita, K., Miyake, Y., Miyamoto, M., Hasegawa, Y., Makino, T., Van der Perre, S., Cousin Saint Remi, J., Van Assche, T., Baron, G.V., 2015. Adsorption and diffusion phenomena in crystal size engineered ZIF-8 MOF. J. Phys. Chem. C 119, 28430–28439.

Thanh, M.T., Thien, T.V., Du, P.D., Hung, N.P., Khieu, D.Q., 2018. Iron doped zeolitic imidazolate framework (Fe-ZIF-8): synthesis and photocatalytic degradation of RDB dye in Fe-ZIF-8. J. Porous Mater. 25, 857–869.

Tsotsalas, M., Maheshwari, H., Schmitt, S., Heißler, S., Feng, W., Levkin, P.A., 2016. Freestanding MOF microsheets with defined size and geometry using superhydrophobic–superhydrophilic arrays. Adv. Mater. Interfaces 3, 1500392.

Wang, J.-W., Li, N.-X., Li, Z.-R., Wang, J.-R., Xu, X., Chen, C.-S., 2016. Preparation and gas separation properties of Zeolitic imidazolate frameworks-8 (ZIF-8) membranes supported on silicon nitride ceramic hollow fibers. Ceram. Int. 42, 8949–8954.

Wankat, P.C., 1991. A review of:"Gas separation technology". Separ. Purif. Rev. 20, 199–200.

Xie, J., Yan, N., Liu, F., Qu, Z., Yang, S., Liu, P., 2014. CO_2 adsorption performance of ZIF-7 and its endurance in flue gas components. Front. Environ. Sci. Eng. 8, 162–168.

Xu, W., Wang, G., Xu, J., Liu, Y., Chen, R., Yan, H., 2019. Modification of diatomite with melamine coated zeolitic imidazolate framework-8 as an effective flame retardant to enhance flame retardancy and smoke suppression of rigid polyurethane foam. J. Hazard Mater. 379, 120819.

Yaghi, O.M., 1997. Crystalline Metal-Organic Microporous Materials. Google Patents.

Yoo, D.K., Bhadra, B.N., Jhung, S.H., 2020. Adsorptive removal of hazardous organics from water and fuel with functionalized metal-organic frameworks: contribution of functional groups. J. Hazard Mater. 403, 123655.

Yuan, J., Li, Q., Shen, J., Huang, K., Liu, G., Zhao, J., Duan, J., Jin, W., 2017. Hydrophobic-functionalized ZIF-8 nanoparticles incorporated PDMS membranes for high-selective separation of propane/nitrogen. Chem. Eng. J. 12, 110–120.

Zhang, C., Dai, Y., Johnson, J.R., Karvan, O., Koros, W.J., 2012. High performance ZIF-8/6FDA-DAM mixed matrix membrane for propylene/propane separations. J. Membr. Sci. 389, 34–42.

Zhang, Y., Jia, Y., Li, M., Hou, L.a., 2018. Influence of the 2-methylimidazole/zinc nitrate hexahydrate molar ratio on the synthesis of zeolitic imidazolate framework-8 crystals at room temperature. Sci. Rep. 8, 9597.

Zhang, H., Shi, X., Li, J., Kumar, P., Liu, B., 2019. Selective dye adsorption by zeolitic imidazolate framework-8 loaded UiO-66-NH_2. Nanomaterials 9, 1283.

Zheng, B., Zhu, Y., Fu, F., Wang, L.L., Wang, J., Du, H., 2017. Theoretical prediction of the mechanical properties of zeolitic imidazolate frameworks (ZIFs). RSC Adv. 7, 41499–41503.

Zornoza, B., Martinez-Joaristi, A., Serra-Crespo, P., Tellez, C., Coronas, J., Gascon, J., Kapteijn, F., 2011. Functionalized flexible MOFs as fillers in mixed matrix membranes for highly selective separation of CO_2 from CH_4 at elevated pressures. Chem. Commun. 47, 9522–9524.

Zou, D., Liu, D., Zhang, J.J.E., Materials, E., 2018a. From zeolitic imidazolate framework-8 to metal-organic frameworks (MOF s). Representative Substance for the General Study of Pioneering MOF Applications 1, 209–220.

Zou, D., Liu, D., Zhang, J., 2018b. From zeolitic imidazolate framework-8 to metal-organic frameworks (MOF s): representative substance for the general study of pioneering MOF applications. Energy Environ. Mater. 1, 209–220.